Effect of a compliant substrate on the rebound of a spherical shell

Théophile Rémond, Vincent Dolique, Renaud G Rinaldi, Jean-Christophe Géminard

Effect of a compliant substrate on the rebound of a spherical shell

Théophile Rémond[1], Vincent Dolique[1], Renaud G. Rinaldi[2], and Jean-Christophe Géminard[1]
[1] *CNRS, ENS de Lyon, LPENSL, UMR5672, 69342, Lyon cedex 07, France*
[2] *MATEIS, CNRS UMR 5521, INSA-Lyon, Univ Lyon, F-69621 Villeurbanne, France*
(Dated: February 3, 2026)

The impact between a spherical shell (a table-tennis ball, in practice) and a compliant silicone surface is studied. Experimentally, the potential for achieving higher reflected angular velocity on a compliant surface compared to a rigid one is explored with special attention given to the roles of friction and of the soft substrate deformability. Additionally, local observations of the contact region and potential buckling of the spherical shell are pursued. In normal incidence, the main effect of the soft substrate on the rebound is a decrease in the coefficient of restitution of the linear velocity and an increase in the duration of contact, without a clear dependence on the substrate thickness. In addition, by observing the shell geometry at contact it was found that the shell flattening prior to its buckling is smaller on a soft surface than that observed on a rigid surface. In oblique incidence, the introduction of a soft layer clearly increases the ability of the substrate to transfer spin to the spherical shell, with a significant dependence on the layer thickness. A mechanical model incorporating linear elasticity of the surface shows a good correlation with the latter experimental results.

I. INTRODUCTION

The impact between objects is an everyday phenomenon that raises many questions ranging from simple kinematics (speeds after vs. speeds before contact) to the possible permanent deformation of the objects, or even their breakage, induced by contact forces. If one wishes to consider collisions involving hollow objects, the simplest case is probably that of a spherical shell striking a rigid plane. There are thus numerous studies on the bounce of a table tennis ball on a rigid and flat surface, as it is a prototypical model of thin-walled spherical shells.

Under normal incidence, without initial spin, it is observed that the shell buckles from a critical flattening of about twice its thickness [1–5]. The friction is then playing a major role in the energy dissipation, leading to a significant decrease of the restitution coefficient of the linear velocity [5, 6].

In oblique incidence, or for shells initially spinning around the normal to the incidence plane, the contact results in a change in the spin. For an impact on a rigid surface, without initial spin, the reflected angular velocity is limited by sliding. Theoretical models have been developed to explain the bounce of spherical shells on a rigid surface [7, 8], giving rise to laws trying to predict the rebound regardless of the initial trajectory [9, 10]. For limited incidence angle, the maximum angular velocity is achieved because the shell leaves the substrate while rolling without sliding [8]. However for more grazing trajectories, the shell still slides as it leaves the substrate because the frictional force is no longer sufficient to achieve rolling without sliding during the contact time.

The above results are valid for spherical shells, of which table-tennis balls are the prototype, bouncing on rigid substrates. Other studies, however, show that, after collision, spin beyond rolling without sliding [10–14] and even, in very specific conditions, normal restitution coefficient greater than 1 [15], can be observed when energy is stored by the impacted surface. In this context, it is crucial to consider the bounce off a deformable surface, as the mechanical properties of the latter become essential for predicting the subsequent kinematics.

The study of the buckling of a spherical shell made of an elastic rubber has already been conducted [1, 14, 16]. Additionally, the buckling of a table tennis ball with a compliant surface has been investigated under quasi-static uniaxial compression [6, 9]. However, these results are marginal and have not been obtained under dynamic loading similar to that considered in the experiments performed with rigid surfaces [5, 8, 9].

Fundamentally, new questions arise compared to what has been determined on a rigid surface. One might think that elastomeric surfaces increase the friction coefficient between the surfaces in contact. Moreover, more energy dissipation may eventually be expected on soft viscoelastic surfaces. Also, one can wonder how the thickness and the deformation of the substrate alter the buckling of the shell from a geometrical point of view, as well as the restitution of speed and spin. Therefore, in this study, normal and oblique impacts of a deformable table tennis ball on compliant surfaces of varying thicknesses will be investigated and then compared to the results obtained on a rigid surface to draw qualitative conclusions. A dense silicone elastomer has been selected to design the compliant surfaces. This choice is motivated by the transparency, which permits the observation of the contact region, and the hyperelasticity of the material.

II. EXPERIMENTAL PRINCIPLE AND SETUP

The aim of the experiment is to assess the role played by the substrate properties in the characteristics of the rebound of a spherical shell. Thus, we propose to probe the reflected linear, $\vec{v}_r$, and rotational, $\vec{\omega}_r$, velocities as well as the rebound angle θ_r for a shell impinging on the substrate with well-defined initial velocities, $\vec{v}_i$ and $\vec{\omega}_i$, and incidence angle, θ_i. Ideally, the experimental setup should make it possible the observation of the deformation of the shell during impact.

A. Trajectory

In order to assess how the collision alters the trajectory, we consider the rebound of a spherical shell moving downwards along the vertical with the linear incident velocity $\vec{v}_i$ which collides with a, nominally flat, solid substrate (Fig. 1). For simplicity, the shell does not initially spin ($\vec{\omega}_i = \vec{0}$). Also, the substrate is tilted and makes the angle α with the horizontal such that the incidence angle, the angle that the incident velocity $\vec{v}_i$ makes with the normal to the surface (z-axis), $\theta_i = \alpha$. For convenience, the y-axis is chosen along the slope such that the x-axis is perpendicular to the incidence plane (y,z). Indeed, considering the symmetry of the problem, we predict that the trajectory will remain in the (y,z) plane.

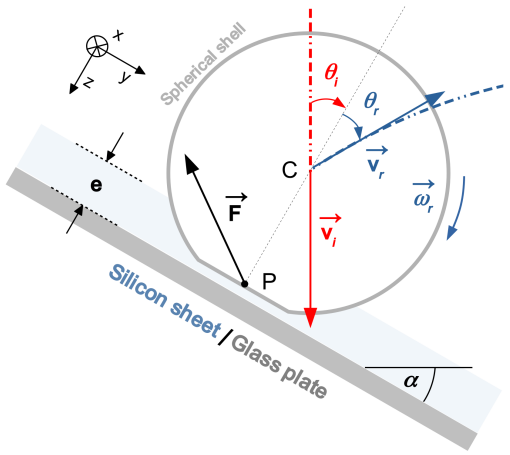

FIG. 1. Sketch of the experimental configuration: the spherical shell reaches the substrate, a glass plate coated with a silicone sheet of thickness e, with the initial velocity $\vec{v}_i$, along the vertical. Initially, the spherical shell does not spin. The nominally flat substrate makes the angle α with the horizontal such that the incidence angle $\theta_i = \alpha$. After rebound, the linear velocity $\vec{v}_r$ makes the angle θ_r with the normal to the surface (z-axis) whereas the spherical shell spins with the rotational velocity $\vec{\omega}_r$ around the x-axis. We denote C the center of the sphere, P the center of the contact region, $\vec{F}$ the force applied by the substrate on the spherical shell.

As it is a prototypical model of thin-walled spherical shell, we perform the experiments with a table-tennis ball. Let us mention that, as a consequence, in the following the term ball will be largely employed and does refer to the "spherical shell" under study. The ball (Cornilleau^{TM}, P-ball 3 stars, 4 cm-in-diameter, mass of 2.7 g, ABS plastic) is launched using a striker mechanism that consists of a metal rod propelled by a compressed spring as already used in [5, 8]. For each experimental test, the system is initially armed by compressing the spring. The ball is then put into place in a holder underneath. In order to achieve reproducible experimental conditions, a special attention is paid to ensure that the ball weld (where the two hemispheres are bonded) is in the horizontal plane. To do so, the weld is previously marked with a dashed line, and the images of each test were screened prior to further post-processing, to validate the weld position. The striker is subsequently released. The ball reaches the substrate with the vertical incident velocity, $\vec{v}_i$, which typically ranges from 1 m s^{-1} to 12 m s^{-1} depending on the initial compression of the spring (the reader should refer to [9] for further details).

Side images of the rebound are captured at a constant frame-rate using a high-speed camera (Kron Technologies, Chronos 2.1-HD, monochrome image sensor, 2,142 fps). The optical axis of the camera is set along the normal to the incidence plane (the x-axis) to keep the whole trajectory in the focal plane (Fig. 2). The position of the ball is determined on each recorded image, using the image analysis software ImageJ [17]. Its velocity $\vec{v}$, before and after the rebound, is estimated as a function of time t by interpolating its successive positions through time t by a parabola. We observe that the ball accelerates downwards due to the acceleration of gravity. The velocities right before, v_i, and after, v_r, the rebound (supposed to be instantaneous at this timescale) are then evaluated at the intersection of the two parabolas, which defines the time of contact t_c. In a similar manner, the rebound angle, θ_r, is estimated at t_c from the interpolation of the trajectory after the rebound. Finally, the rotational speed ω_r around the x-axis is evaluated by considering in the images the orientation through time t of the dashed line marking the ball joint.

B. Deformation of the ball shell at contact

The substrate consists of a glass plate covered with a layer of a highly elastically deformable material (Fig. 1). The material used in the study is a transparent RTV silicone rubber (Loctite, SI 595). This material is an elastomer which exhibits an almost ideal hyperelastic behavior at room temperature. The layer is prepared by leveling, with a sharp blade guided by two spacers, the liquid silicone initially poured onto the glass plate. The substrate is then rested overnight at room temperature to complete the curing prior to any experimental test. Various sets of spacers are used to tune the thickness of the elastic layer. We report in Table I the thickness e of each sample measured after curing.

Sample name	e1	e2	e3	e4
Thickness e ($\pm$ 0.03 mm)	0.50	0.96	1.25	1.78

TABLE I. Thickness of the silicone layer (samples e1 to e4).

As already evoked, we specifically choose a transparent silicone which makes it possible to observe from below the contact region between the ball and the substrate during the impact. Results obtained in the case of a rebound in normal incidence (α = 0 deg.) on a rigid surface have been previously reported [5, 9]. The shadow of an array of parallel needles is cast from underneath on the ball surface. By observing the contact region from a side view at a 45 deg angle, as depicted in Fig. 3, one can assess the deformation of the ball shell from the distortion of the needles shadows. For practical reasons, when observing the contact region, we use the same camera as that used for the observation of the trajectory, whose posi-

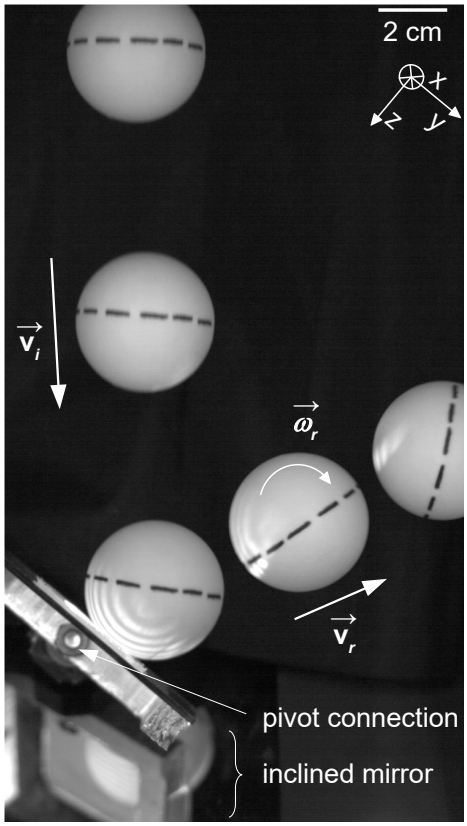

FIG. 2. Superimposed images of the ball colliding with the tilted substrate. For the sake of clarity, only five images, with a time difference of 7.9 ms between two consecutive images, are shown here (frame rate: 2,142 fps). The position of the ball through time, previous to the collision, is used to assess the incident velocity, v_i = 9.8 m s^{-1}. The position of the ball through time, after the collision, is used to assess the outcoming linear velocity, v_r = 5.8 m s^{-1} and the rebound angle $\theta_r = 24$ deg. The black dashes drawn onto the ball to mark the ball joint are used to assess the rotational velocity around the x-axis after the rebound, ω_r = 302 rad s^{-1} [α = 45 deg, $e = 0.96$ mm].

tion remains unchanged. A mirror making a 22.5 deg angle with the horizontal is used to provide a view at 45 deg from below without moving the camera. Focus is made on the image in the mirror of the region of interest, and the frame-rate is set to 19,784 fps offering a decent compromise between the temporal and the spatial resolutions. With a contact duration of about 0.5 ms, around 10 images are captured during the contact between the ball and the substrate.

In practice, a powerful LED (Luxeon Rebel ES, LXML-PWN2, 230 lm) and a lens are used to cast the shadow of the array of equally-spaced steel needles aligned along the y-axis (Fig. 4). The use of the array clears any imprecision that might be due to the relative position of the shadow of a single needle with respect to the impact region. Ultimately, the shadow experiencing the largest geometrical change is the closest to the center of the contact region. We shall thus consider only

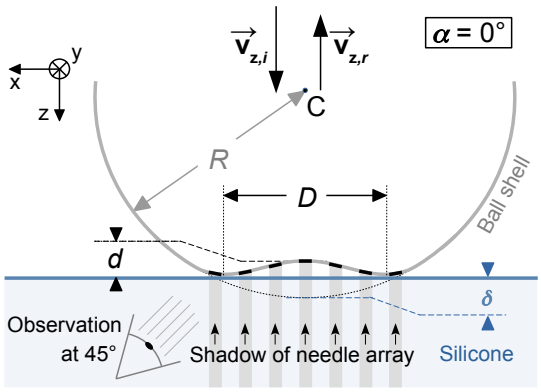

FIG. 3. Sketch of the ball in contact with the substrate ($\alpha = 0$ deg). The shadow of an array of parallel needles (aligned with the y-axis) is casted on the ball surface (black dashes). The surface is observed from below at a view angle of 45 deg. From the images of the deformed array (Fig. 4), one can determine the buckling depth d and the diameter of the deformed region D.

that shadow to determine the relevant geometrical characteristics such as the depth d and diameter D of the buckled region (Fig. 3).

III. EXPERIMENTAL RESULTS

A. Focus on the contact region in normal incidence

In a first step, we focus on the local deformation of the ball shell for normal impacts at incident velocities $v_{z,i}$ ranging from 1 to 12 m s^{-1} onto the different soft surfaces of various thicknesses. As an example, we display in Fig. 4, a series of images obtained for the impact on a 0.96 mm thick substrate (Sample e2) at normal velocity $v_{z,i}$ = 12.7 m s^{-1}. Qualitatively, during the collision, the diameter D of the contact region first increases, reaches a maximum and then decreases until the ball loses contact with the substrate. As previously observed for a collision with a rigid surface, the contact region between the ball and the silicone substrate exhibits a reversible transition from a flat disk to a ring, with a buckled central part, for normal velocities above a critical velocity of about $v^c_{z,i}$ = 5 m s^{-1} [5].

Now based on the analysis of the distortion of the shadows of the needles (see Sec. II B), the evolution of the depth d and diameter D of the contact region through time can be quantified for various samples and incident velocities. Reporting in Fig. 5 the depth d as a function of the diameter D, we observe that the curves obtained during the increase or decrease almost overlap for all the substrate thicknesses and incident velocities in the experimental range. Thus, unlike the collision onto a rigid surface, the system does not exhibit any significant hysteresis [5]. The deformability of the substrate reduces significantly the effects of the solid friction that explains the

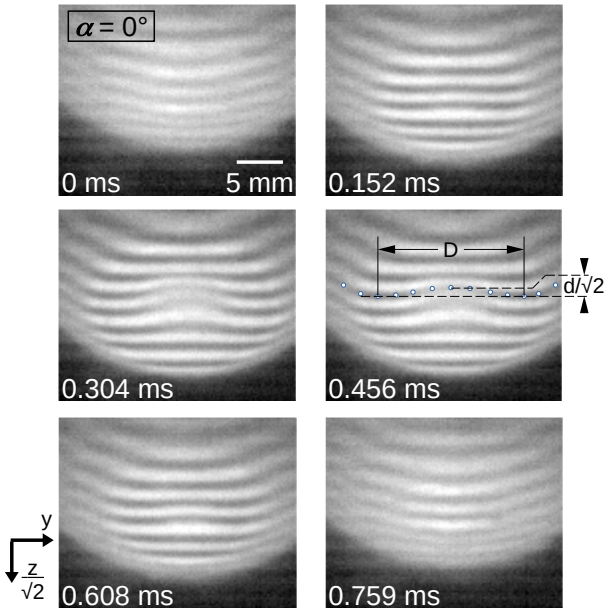

FIG. 4. Sequence of images showing the deformation of the ball shell during the collision with the soft transparent substrate, in normal incidence. We report here only one out of three captured images. The shadow of the array of parallel needles, visible as dark lines in the image, makes it possible to assess the profile of the ball shell in contact with the substrate. In this sequence, one can clearly observe that the shell is subjected to a buckling instability. Indeed, the curvature of the needle shadow inverts at the center marking an inversion of the local curvature of the shell [$v_{z,i}$ = 12.7 m s^{-1}, α = 0 deg, e = 0.96 mm, Sample e2, frame rate: 19,784 fps].

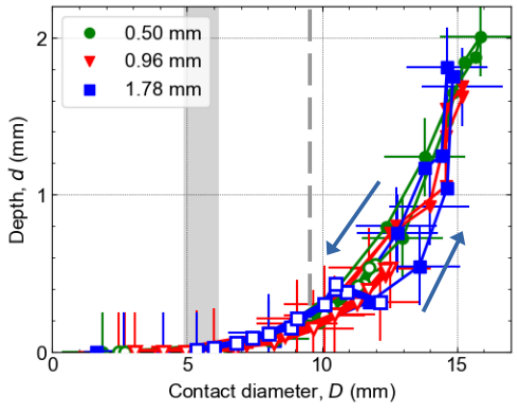

FIG. 5. Depth of the buckle d as a function of the diameter of the contact region D during the contact, for various thicknesses e of the silicone layer and incident velocity v_i (Open symbols: v_i = 8 m s^{-1}, Full symbols : v_i = 13 m s^{-1}). Unlike what is observed on a rigid surface, the curves upon loading and unloading (arrows) almost overlap. The gray and vertical dashed line indicates the theoretical diameter of the contact at the buckling onset (of about 9 mm [2]) whereas the vertical gray region marks the actual buckling onset [$\alpha = 0$ deg].

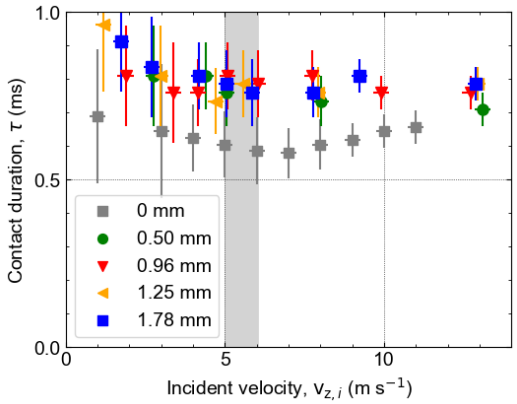

FIG. 6. Duration of the contact τ as a function of the incident velocity $v_{z,i}$. In the whole experimental range of thicknesses e of the silicone layer, the duration τ of the contact is larger for the rebound on the deformable substrate than on the rigid one (gray squares from Ref. [5]). Prior to the buckling instability (vertical gray line), the duration τ decreases when the incident velocity $v_{z,i}$ is increased, whereas a plateau or a slight increase of τ is observed beyond.

hysteretic behavior of the ball shell buckling when the ball collides with a solid surface.

Also, we observe in Fig. 5 that the depth d starts increasing for a contact diameter D smaller than predicted theoretically for a contact with a solid substrate [2]. Thus, whatever the testing condition, the ball is seen to buckle earlier on a compliant surface compared to what is observed on a rigid surface [5]. Two phenomena, yet to be proven, can be evoked to explain this finding: first, due to significantly less friction during contact with a compliant surface, the onset of the buckling instability is not delayed. Second, when the ball impacts the substrate, the latter, being deformable, can exert pressure and push to raise the shell upwards at the center, favoring its buckling.

Focusing on the contact region also makes it possible to estimate the duration τ of the contact by counting the number of frames in which the diameter of the contact region D is greater than zero. In Fig. 6, we display τ as a function of the incident normal velocity $v_{z,i}$. Whatever the thickness e, the data follow the same trend: prior to buckling (evidenced, for the case of the rigid substrate, by the gray vertical line) a significant decrease of τ when the incident velocity is increased followed, beyond the buckling instability, by a plateau or a slight increase of τ. However, we observe that the duration of the contact is systematically larger for collisions with the deformable substrate than for collisions with the rigid one. This experimental observation is not surprising and might be accounted for by the combination of two contributions: first, one must consider that during the contact the ball travels almost back and forth through the layer thickness which adds a contribution of the order of $2e/v_{z,i}$ to the contact duration. With a typical thickness e of the order of 1 mm and a typical incident velocity of the order of 5 m s^{-1}, this contribution is of the order of 0.2 ms (the velocity cancels out during the con-

tact). Second, one can consider the ball-substrate ensemble as a spring-mass system. The collision duration is half the period of the system. The silicone layer decreases the stiffness of the system whereas the mass remains unchanged, which leads to the increase of the characteristic time of the system, thus of τ. If both arguments can qualitatively explain that τ is larger when a silicone layer is introduced, the measurements do not reveal, in the whole experimental range, any systematic dependence of τ on the thickness e of the layer. Yet, it is worth noting that the measurement precision, illustrated by the error bars in the figure, hinders to definitively conclude that τ does not depend on neither the thickness e nor the velocity v_i. However, at this point, it is worth comparing the apparent stiffness of the layer to that of the ball. From [5], we estimate that the apparent stiffness of the ball is of about $k_b \simeq 6\,10^4$ N m^{-1} which leads, with $m_b = 2.7$ g to the estimate of the contact time $\tau \simeq 0.6$ ms in accordance with the experimental measurements for a solid substrate. For the elastomer coating, we estimate for a typical diameter of the region of contact of the order of 1 cm, for a typical thickness of the order of 1 mm and for a typical Young modulus (later estimated in this paper) of 3 MPa, that the apparent stiffness of the layer is of about $k_s \sim 2.5\,10^5$ N m^{-1}, thus significantly larger than k_b. Provided that these estimates are correct, the spring-mass model shows that the contact time is mainly governed by the stiffness of the ball and not that of the substrate. The dependence on the thickness is thus expected to be weak, at least for thin coatings.

In the next section, we observe the rebound of the ball at a larger scale while varying the incidence angle and assess the ability of the substrate to transfer velocity and/or spin to the ball depending on the thickness of the silicone deformable layer.

B. Ball trajectory

1. *Restitution of the normal component of the velocity*

Still considering the case of a ball impinging in normal incidence onto the horizontal glass plate coated with a layer of silicone, we focus on the restitution of the incident linear normal velocity, $v_{z,i}$. To do so, we define the normal restitution coefficient $\varepsilon_z \equiv -v_{z,r}/v_{z,i}$, the ratio of the reflected normal velocity $v_{z,r}$ to the incident normal velocity $v_{z,i}$. In Fig. 7, we report ε_z as a function of $v_{z,i}$ for rigid and deformable samples.

On the one hand, we observe two regimes on both sides of a critical velocity of about 5 m.s^{-1} which, we remind, corresponds to the buckling instability, as we know from a previous study [5]: at small incident velocities, a plateau of the restitution coefficient ε_z is observed whereas ε_z decreases when the velocity $v_{z,i}$ is further increased and the ball buckles.

On the other hand, we observe that ε_z is systematically smaller by about 10% or more for the rebound of the ball on the soft substrate than on the bare rigid one. We note that the data obtained for distinct layer thickness e do not strictly superimpose but the experimental setup does not make it possible to study the dependence on the thickness in detail.

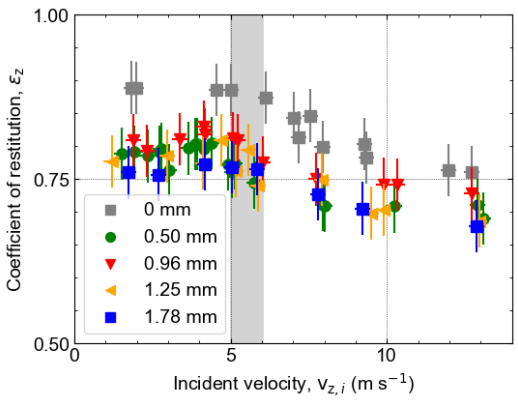

FIG. 7. Normal restitution coefficient ε_z as a function of the normal incident velocity $v_{z,i}$ for various thicknesses, e, of the silicone layer. As for the collision with a solid surface, we observe two regimes on both sides of a critical velocity of about 5 m s^{-1} (vertical gray line) which is associated with the buckling of the ball shell. The main observation is that the restitution is systematically smaller when the solid substrate is coated with a silicone layer.

In summary, in normal incidence, both the duration of the contact, τ (Sec. III A) and the restitution coefficient of the incident normal velocity, ε_z, differ between the rigid and the soft substrates we studied.

It is worth commenting here that the limit $e \to 0$ is nevertheless singular. Indeed, coating the solid substrate, whatever the thickness e of the elastomer layer, is crucial as it changes the frictional properties of the surface. However, we know from our previous studies that the friction plays an important role in the dissipation during the contact, even in normal incidence [5, 8]. Yet, the dependence of τ and ε_z on the incident velocity, $v_{z,i}$, or on the silicone-layer thickness, e, remains weak and are poorly accessible to our experimental device.

In the next Section III B 2, we shall see that, by contrast, the elasticity of the silicone layer is predominant in the ability of the substrate to transfer spin to the ball.

2. *Spin transfer for oblique incidence*

We now consider the configuration in which the ball reaches an inclined substrate. In this situation the tangential velocity is finite and a significant shear force is applied to the soft surface which, in turn, transfers spin to the ball. Experimentally, we tilted the substrate at angles ranging from 0 to 60 deg and, performing the same initial launches, we tracked the resulting ball trajectories.

In Fig. 8 we report, for various thicknesses e of the silicone layer, the reflected angular velocity of the ball as a function of the tangential incident velocity $v_{y,i}$. In the whole experimental range, $v_{y,i} \in [0, 10]$ m s^{-1}, we observe that the reflected rotational velocity $\omega_{x,r}$ is always larger for a bounce on a soft substrate than on a solid one. Moreover, the experimental results

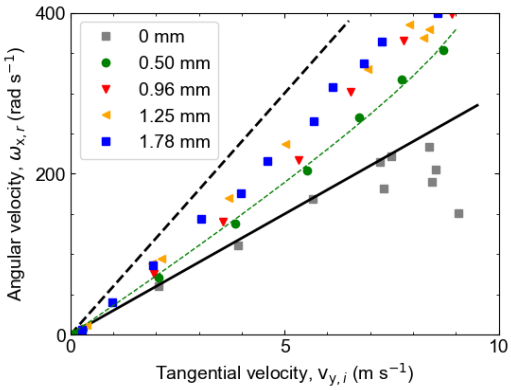

FIG. 8. Reflected rotational velocity $\omega_{x,r}$ as a function of the initial tangential velocity $v_{y,i}$ for a collision in oblique incidence without initial spin. The green dashed line is the interpolation of the experimental data obtained for $e = 0.5$ mm by the model proposed in Sec. IV A. The solid black line represents the lower bound, which corresponds to a ball rolling without sliding as it leaves the substrate [$\Sigma = 0$, Eq. (10)]. The dashed black line corresponds to the theoretical upper bound corresponding to the case in which the initial tangential velocity of the contact point would be reversed [$\Sigma = -1$, Eq. (10)].

reveal a clear dependence on the thickness e of the silicone layer, an increase in the thickness leading to an increase of the final spin.

For a rigid substrate, *i.e.* the gray squares in Fig. 8, regardless of the initial conditions provided that the tangential velocity is not too large, the maximum reflected angular velocity $\omega_{x,r}$ corresponds to the case of a ball leaving the substrate while rolling without sliding [8]. Yet, the reflected rotational velocity is seen to depart from this prediction, becoming smaller, when the frictional force is no longer sufficient to prevent the sliding between the ball and the rigid surface before the ball leaves the surface. This is the case in Fig. 8 for $v_{y,i}$ typically greater than 8 m s^{-1}.

Now focusing on the soft silicone substrates, the large reflected rotational velocities that are achieved experimentally suggest that the tangential velocity of the contact region with respect to the substrate must change in sign, thus overcoming the limits imposed by the condition of rolling without sliding. In the forthcoming section, the final rotational velocity will be accounted for by a simplistic model involving the lateral elasticity of the impacted surface.

IV. THEORETICAL ANALYSIS

A. Modeling

For the sake of simplicity, following the approach suggested by Cross [12], we model the soft surface as a cart that translates along the substrate surface as depicted in Fig. 9. The ball lands on top of the cart, of mass m_c, which is attached to the solid surface through a spring of stiffness k and damping coefficient η. We also consider the ball as a spherical shell, of a mass m_b, that does not deform during the collision. We denote v_i and v_r its incident and reflected velocities respectively and ω_r the reflected rotational velocity. We remind that the ball does not initially spin. The incident and reflected velocities make respectively the angles θ_i and θ_r with the normal to the surface. From now on, one must consider that the rebound of the ball occurs in several stages.

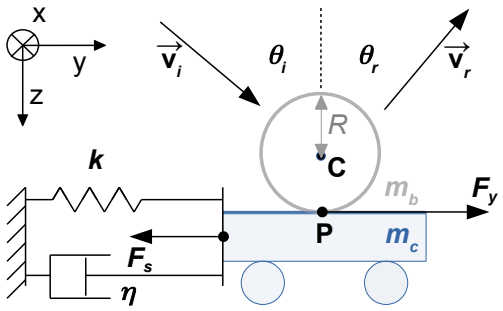

FIG. 9. Schematic representation of the model used to describe the rebound in oblique incidence of a ball on a soft surface. The ball of mass m_b hits the cart of mass m_c with the incident velocity $\vec{v}_i$. During the contact the ball applies to the cart the force F_y along the y-axis. Conversely, the cart applies the force $-F_y$ which reduces the tangential velocity of the ball and puts the latter in rotation. In response to the displacement of the cart, the spring exerts the restoring force $F_s = -kY - \eta \frac{dY}{dt}$.

Initially, when the ball makes contact with the cart, it necessarily starts sliding, which reduces its tangential velocity while carrying the cart away tangentially. During this first stage, the ball and the cart are in frictional contact. Consequently, the ball exerts the tangential force $F_y = \mu |F_z|$ along the y-axis where F_z is the normal component of the contact force and μ is the dynamic friction coefficient. The position Y of the cart is governed by the dynamical equation:

$$m_c \frac{d^2Y}{dt^2} + \eta \frac{dY}{dt} + kY = F_y. \tag{1}$$

and, simultaneously, the tangential velocity of the ball is governed by:

$$m_b \frac{dv_y}{dt} = -F_y. \tag{2}$$

The force F_y is thus associated with a torque that makes the ball spin according to:

$$J \frac{d\omega_x}{dt} = R F_y \tag{3}$$

where $J = \frac{2}{3} m_b R^2$ is the moment of inertia of a spherical shell. The friction between the two surfaces leads to a decrease of the relative velocity v_P of the contact point P which is given by:

$$v_P = v_y - R\,\omega_x - \frac{dY}{dt}. \tag{4}$$

The first stage ends if the frictional force is large enough for v_P to cancel out during the contact time τ.

The second stage starts when the condition of rolling without sliding, $v_P = 0$, is reached. During this second stage, the dynamics of the ball and slider are constrained by:

$$v_y - R\,\omega_x = \frac{dY}{dt}. \tag{5}$$

In addition, the equations of dynamics applied to the ball impose a relationship between the variations of the velocity v_y and the rotational velocity ω_x:

$$J\,\frac{d\omega_x}{dt} = -m_b R\,\frac{dv_y}{dt}. \tag{6}$$

Combining Eq. (5) and the dynamical equations for the ball motion, we get:

$$F_y = -\frac{2}{5}\,m_b\,\frac{d^2Y}{dt^2} \tag{7}$$

and then the equation governing the dynamics of the cart during the rolling without friction:

$$\left(m_c + \frac{2}{5}\,m_b\right)\frac{d^2Y}{dt^2} + \eta\,\frac{dY}{dt} + kY = 0. \tag{8}$$

The second stage lasts as long as the magnitude of the normal force, $|F_z|$, is large enough to ensure that the point P does not slide.

Indeed, the magnitude of the normal force $|F_z|$ decreases before the ball leaves the substrate. Thus, the magnitude of the tangential component $|F_y|$ necessarily overcomes the onset of sliding $\mu_s\,|F_z|$, where μ_s is the static friction coefficient, before the end of the contact. During a third stage, the dynamics of the system is similar to that of the first stage. In practice however, the static frictional coefficient μ_s is greater than μ, the relative velocity of the two surfaces in regard is initially zero and the magnitude of the normal force $|F_z|$ is small and decreasing fast, so that we expect the duration and the effects of this third stage on the dynamics of the ball to be negligible.

Thus, we solve numerically the system taking into account the first and second stages, only. The first stage of the collision provides the initial conditions for solving Eq. (8). The ball leaves the surface at time τ with a reflected rotational velocity $\omega_{x,r}$ and a linear tangential velocity $v_{y,r}$ that depend on the velocity of the cart at the end of the second stage. If the cart ends up at time τ in the elastic return phase of its sinusoidal trajectory, meaning it has a reversed velocity in the y direction, the rotational velocity of the ball is larger than that obtained on a rigid surface [Eq. (5) with $\frac{dY}{dt} < 0$ instead of being 0].

B. Adjustment to the experimental data

The aforementioned theoretical framework allows the prediction of the reflected angular velocity as a function of the ball incident trajectory provided that the parameters of the model are known. The prediction relies on several material constants and/or adjustable parameters. The mass of the ball, $m_b = 2.7$ g, and its radius $R = 2$ cm are known. Thus, its moment of inertia $J = \frac{2}{3}\,m_b R^2$ is also given. By contrast, the mass of the cart m_c, the stiffness k, the damping coefficient η as well as the frictional coefficient, μ, are unknown.

In addition, the model does not describe the dynamics along the normal to the surface (z-axis), which requires making additional assumptions. However, from the data in Fig. 6, we can set the duration of the contact $\tau = 0.8$ ms. In the same way, from the data in Fig. 7, we set the restitution coefficient, $\varepsilon_z = 0.8$. The duration τ imposes the duration of the integration of the model whereas ε_z is used to get an estimate of the average normal force, $F_z = (1+\varepsilon_z)\,m_b\,v_{z,i}/\tau$.

The frictional coefficient μ governs the coupling between the normal, F_z, and the tangential, F_y, components of the reaction force between the ball and the substrate. We solve the set of equations above, assuming for the sake of simplicity that the normal force is constant and equal to its average over the contact time. The model is found to adjust correctly to the experimental data with a constant frictional coefficient of about $\mu \sim 0.92$, independent of the silicone layer thickness (Fig. 8). The frictional coefficient was found to be around 0.2 for the contact between the ball and a rigid glass plate [5]. The value around 1 is here compatible with the large value of the frictional coefficient measured for the contact of the ball with rubber coating [18]. Let us comment here that sliding friction tests giving an independent estimate of the frictional coefficient are barely feasible in the range of sliding velocities implied here (a few $\mathrm{m\,s^{-1}}$, typically). Note that a large value of μ ensures that the rolling without sliding condition is reached rapidly, even for large incident angle. Thus, contrary to what is observed for glass for which the data depart from the linear law for $v_{y,i} \sim 8\ \mathrm{m\,s^{-1}}$ (thus for θ_i of the order of 55 deg), no drastic change in regime is observed on the data obtained with the soft substrate. The rolling without sliding condition is reached in the whole experimental range which is compatible with a large enough value of μ (typically larger than 0.8), only. In addition, we checked that taking $\mu = 0.8$ instead of $\mu = 0.92$ leads to a decrease by 2% of the estimate of the stiffness k.

Likewise, the experimental data are also correctly accounted for taking $\eta = 0$, which suggests that the viscous dissipation does not play any significant role in the ability of the tangential motion of the silicone layer to transfer momentum to the ball.

Finally, the interpolation of the experimental data leads to an almost constant mass of the cart $m_c \sim 0.6$ g whereas, by contrast, only the tangential stiffness k significantly depends on the thickness e of the silicone layer, the latter decreasing when e is increased (Table II). If the decrease of the stiffness k associated with an increase of the thickness e is intuitively expected, the constant mass m_c of the cart is surprising. We attempted to adjust the whole set of data imposing both an increase of the m_c and a decrease of k but the best adjustment is obtained by taking m_c constant. This result remains unexplained but one can however notice that the layer is crushed during the process and that the model, which remains simplistic, can probably not account for the complexity of the whole

e_s (mm)	0.50	0.96	1.25	1.78
k (10^4 N m^{-1})	4.8	4.0	3.7	3.2

TABLE II. Stiffness k obtained by interpolation of the reflected rotational velocity $\omega_{x,r}$ as a function of the initial tangential velocity $v_{y,i}$ in Fig. 8. Values of k are determined to within 10^3 N m^{-1} [$m_b = 2.7$ g, $R = 2$ cm, $\tau = 0.8$ ms, $\varepsilon_z = 0.8$, $\eta = 0$, $\mu = 0.92$].

phenomenon.

It remains that our simplistic model succeeds in predicting that the silicone layer can achieve larger rotational velocity than a solid substrate (Fig. 8). Moreover, the interpolation of the experimental data makes it possible to reveal which is the most relevant parameter and its dependence on the layer thickness, which will be discussed in the next section.

V. DISCUSSION

The calibration of our model with the experimental data reveals that the apparent stiffness k of the spring increases when the thickness e of the substrate is decreased. The spring is introduced in the model to account for the tangential stiffness of the substrate, relative to the displacement of its free surface in the direction parallel to the surface plane, thus to shear. The stiffness k can thus be directly related to the shear modulus G of the material. Considering that the ball is in contact with the silicone layer over a surface area S, we can write:

$$G \approx \frac{k\,e}{S}. \tag{9}$$

Considering further that the contact region is a disk of typical diameter $D \approx 10$ mm (Fig. 5), we obtain that $G \sim 0.5$ MPa and, thus, a Young modulus of the order of 1.5 MPa, consistent with data reported in the literature for unfilled elastomeric materials [19].

Due to the finite stiffness of the substrate, the reflected rotational velocity $\omega_{x,r}$ can be, as observed in Fig. 8, larger than would be observed for a rigid substrate. From our crude theoretical analysis, we understand that this feature is accounted for by the fact that the contact point P (Fig. 9) is likely to move backwards before the ball leaves the surface. Thus, a convenient way to rationalize our experimental data is to introduce the restitution coefficient of the velocity of the contact point P, *i.e.*

$$\Sigma = \frac{v_{y,r} - R\,\omega_{x,r}}{v_{y,i} - R\,\omega_{x,i}}. \tag{10}$$

Defined as is, $\Sigma = 1$ if the point P only slides along the surface without any change of the tangential velocity v_y, $\Sigma = 0$ if the ball leaves the surface while rolling without sliding, and $\Sigma = -1$ if the velocity of the point P is inverted as result of the collision. These last two limits are displayed in Fig. 8 as the solid and dashed black lines respectively. It is then of particular interest to display Σ as a function of the normal incident velocity $v_{z,i}$ to perceive any potential effect of the normal loading. In Fig. 10, we observe a significant dependence of

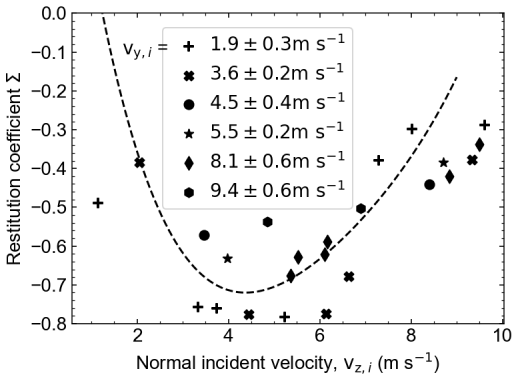

FIG. 10. Coefficient of restitution, Σ, of the velocity of the contact point P as a function of the normal incident velocity of the ball, $v_{z,i}$. The tangential velocity $v_{y,i}$ is fixed for each series of measurements to assess the influence of the normal load, which is not considered in the mechanical model. The dashed line is only a guide for the eye [$e = 0.96$ mm].

Σ on $v_{z,i}$, at constant incident velocity v_i. More precisely, Σ should start from 1 for $v_{z,i} \to 0$ (the frictional force vanishes in this limit) and reach 0 in the limit $v_{z,i} \to \infty$ (the elastomer is crushed which impedes any tangential motion). Between these two expected limits, we observe experimentally that Σ exhibits a minimum, roughly $\Sigma \approx -0.7$, for a normal incident velocity of about $v_{z,i} = 5$ m s^{-1} or less.

Interestingly, this minimum can be predicted theoretically. Indeed, considering that the maximum rotational velocity is achieved if the ball leaves the substrate after exactly half a period of the cart motion governed by Eq. (8), one can estimate Σ considering the initial amplitude of the cart motion as a result of the first stage. Thus, solving first Eq. (1) and then Eq. (8) when rolling without friction is reached, we get:

$$\Sigma_{min} = -\frac{2\,m_b}{2\,m_b + 5\,m_c} \tag{11}$$

With the experimental values of m_b and m_c, we get $\Sigma_{min} \simeq -0.64$ in reasonable agreement with the experimental value observed in Fig. 10 given the scatter of the data.

It is then of particular interest to compare the half-period of the motion of the cart rolling without sliding to the contact duration τ. From Eq. (8), we have:

$$\frac{T}{2} = \pi \sqrt{\frac{m_c + \frac{2}{5} m_b}{k}} \tag{12}$$

For a stiffness $k \simeq 4\,10^4$ N m^{-1} (Table II, $e = 0.96$ mm), we get that $\frac{T}{2} \approx 0.64$ ms, thus close to but smaller than the contact duration $\tau \approx 0.8$ ms reported in Fig. 6. However, it is not surprising that the estimate of $\frac{T}{2}$ is smaller than τ by a few tenths of millisecond. Indeed, taking into account the duration of the first stage during which the ball slides, we rather expect $\tau_s + T/2 = \tau$ where, we remind, τ_s is estimated to range from 60 to 300 μs.

Despite the difficulty to correctly estimate the duration of the successive stages, our experimental results suggest that the largest rotational velocity $\omega_{x,r}$ (minimum Σ) is achieved when the half-period of the spring-mass system $\frac{T}{2}$ compares with the contact duration τ such that the velocity of the contact point P is maximum when the ball leaves the substrate.

VI. CONCLUSION AND PERSPECTIVE

In conclusion we reported on the rebound of a spherical shell (a table-tennis ball) on a nominally flat substrate coated with a mm-thick elastomeric layer. We observed that the coating permits the ball to achieve large final rotational velocities that were not achievable for rebounds on solid substrates [5, 8]. For a soft substrate, which is compliant in shear, the contact region can move backwards in the plane of the substrate when the ball leaves the substrate, which in turn can result in an additional contribution to the ball rotation. The efficiency of the mechanism depends on the layer thickness. The use of a transparent substrate made it possible to observe the contact region and to report on the contact duration, slightly larger than that measured for a rigid substrate. The analysis of the ball motion also shows that the normal restitution coefficient of the velocity is slightly reduced.

The impact of the spherical shell on a compliant surface can be considered as a simplified version of the impact of the ball on a table-tennis racket. Therefore, applied to the table tennis, these results can be useful for a competitor who wants to gain a better understanding of its racket response and assess the amount of spin and speed he can impart to the ball. A natural extension of the present work is thus to get closer to the real substrate by considering the effects of both the architecture and the intrinsic material properties. More precisely, table tennis coverings consist of a foam layer stacked with an elastomeric dense layer covered with an array of cylindrical pimples. The role played by the pimples (both its pattern and geometry) and the elastomer mechanical property will be the subject of a forthcoming study focusing on the applications to table tennis.

ACKNOWLEDGMENTS

TR gratefully acknowledges the financial support from the GDR Sport & Activité Physique. The authors would also like to thank F. Vittoz for setting up the experimental device.

[1] R. Sahli, J. Mikkelsen, M. S. Boye, M. A. Dias, and R. Aghababaei, Frictional contact of soft polymeric shells, arXiv preprint arXiv:2401.14926 (2024).
[2] L. Pauchard and S. Rica, Contact and compression of elastic spherical shells: the physics of a 'ping-pong' ball, Philosophical Magazine B-Physics of Condensed Matter Statistical Mechanics Electronic Optical and Magnetic Properties **78**, 225 (1998).
[3] R. Kitching, R. Houlston, and W. Johnson, Theoretical and experimental-study of hemispherical shells subjected to axial loads between flat plates, International Journal of Mechanical Sciences **17**, 693 (1975).
[4] R. Shorter, J. D. Smith, V. A. Coveney, and J. J. C. Busfield, Axial compression of hollow elastic spheres, Journal of Mechanics of Materials and Structures **5**, 693 (2010).
[5] T. Rémond, V. Dolique, F. Vittoz, S. Antony, R. G. Rinaldi, L. Manin, and J.-C. Géminard, Dynamical buckling of a table-tennis ball impinging normally on a rigid target: Experimental and numerical studies, Physical Review E **106**, 10.1103/physreve.106.014207 (2022).
[6] R. G. Rinaldi, L. Manin, C. Bonnard, A. Drillon, H. Lourenco, and N. Havard, Non linearity of the ball/rubber impact in table tennis: experiments and modeling, Procedia engineering **147**, 348 (2016).
[7] H. Brody, That's how the ball bounces, The Physics Teacher **22**, 494 (1984).
[8] T. Remond, V. Dolique, R. G. Rinaldi, and J.-C. Geminard, Oblique impact of a buckling table-tennis ball on a rigid surface, PHYSICAL REVIEW E **107**, 10.1103/PhysRevE.107.055007 (2023).
[9] T. Rémond, *Physique du rebond: application à la balle de tennis de table*, Ph.D. thesis, Ecole normale supérieure de lyon-ENS LYON (2023).
[10] A. Nakashima, Y. Ogawa, Y. Kobayashi, and Y. Hayakawa, Modeling of rebound phenomenon of a rigid ball with friction and elastic effects, American Control Conference **31**, 1410 (2010).
[11] N. Maw, J. Barber, and J. Fawcett, The oblique impact of elastic spheres, Wear **38**, 101 (1976).
[12] R. Cross, Grip-slip behavior of a bouncing ball, American Journal of Physics **70**, 1093 (2002).
[13] R. Cross, Measurements of the horizontal coefficient of restitution for a superball and a tennis ball, American Journal of Physics **70**, 482 (2002).
[14] R. Cross, Impact behavior of hollow balls, American Journal of Physics **82**, 189 (2014).
[15] M. Y. Louge and M. E. Adams, Anomalous behavior of normal kinematic restitution in the oblique impacts of a hard sphere on an elastoplastic plate, Physical review E **65**, 021303 (2002).
[16] R. Cross, The bounce of a ball, American Journal of Physics **67**, 222 (1999).
[17] W. Schneider, C.A. Rasband and K. Eliceiri, Nih image to imagej: 25 years of image analysis, Nature Methods **9**, 671 (2012).
[18] Y. Wu, A. Varenberg, and M. Varenberg, Table tennis: Effect of humidity on racket rubber tribology, TRIBOLOGY LETTERS **69**, 10.1007/s11249-021-01404-2 (2021).
[19] A. M. Stricher, R. G. Rinaldi, C. Barres, F. Ganachaud, and L. Chazeau, How i met your elastomers: from network topology to mechanical behaviours of conventional silicone materials, RSC ADVANCES **5**, 53713 (2015).